Experiments in Fluids 23 (1997) 20–28

The effect of a discrete window offset on the accuracy of cross-correlation analysis of digital PIV recordings

J. Westerweel, D. Dabiri, M. Gharib

Abstract This paper describes how the accuracy for estimating the location of the displacement-correlation peak in (digital) particle image velocimetry (PIV) can be optimized by the use of a window offset equal to the integer-pixel displacement. The method works for both cross-correlation analysis of single-exposure image pairs and multiple-exposure images. The effect is predicted by an analytical model for the statistical properties of estimators for the displacement, and it is observed in the analysis of synthetic PIV images of isotropic turbulence, and in actual measurements of grid-generated turbulence and of fully-developed turbulent pipe flow.

1 Introduction

The correlation analysis in an interrogation sub-image in particle image velocimetry (PIV) yields an estimate $\hat{u}$ for the displacement of the particle-images within the interrogation region. The measured displacement $\hat{u}$ can be written as

$$\hat{u} = u + \varepsilon \tag{1}$$

where u is the true displacement, and ε the measurement noise, which represents uncertainties due to the finite number of samples (i.e., the number of particle images within the interrogation region, and the number of pixels by which the interrogation region is discretized) that are available for the estimation of u; here all other possible sources of error (e.g., out-of-plane motion, optical aberrations, or inhomogeneous illumination) are considered to be of minor importance, and are ignored in this paper.

Adrian (1991) conjectured that the variation of ε is directly proportional to the particle-image diameter (d_τ), which was actually confirmed in a study by Prasad et al. (1992). The same behavior can be observed in Fig. 1, which shows the results from Monte Carlo simulations for the root-mean-square (RMS) error in pixels (px) of the displacement estimated with the so-called 'three-point Gaussian peak fit' (Willert and Gharib 1991; Westerweel 1993a, b) as a function of the actual displacement (u), also in px, for two different particle-image diameters: note that variation of the measurement error increases for increasing d_τ. Also note that the variation of the measurement error is practically independent of the displacement, except for small displacements, i.e. $|u| < \frac{1}{2}$ px; for this region the variation of the measurement error appears to be directly proportional to u.

This characteristic behavior was also found by Willert and Gharib (1991) in calibration measurements of uniformly displaced test images. The behavior of the RMS value of ε as a function of u is described quite well by an analytical result found by Westerweel (1993a, b), which is also plotted in Fig. 1.

The immediate thought that arises when we observed the result in Fig. 1 is whether we can make use of the behavior of the measurement error for small u to improve the precision of PIV measurements. Actually, this improvement can be obtained quite easily.

For the cross-correlation analysis of a pair of single-exposure digital PIV images it is relatively simple to offset the interrogation windows by the integer part of the particle-image displacement. Hence, the residual displacement is only the fractional amount of the particle-image displacement (in pixel units), which is always smaller than $\frac{1}{2}$ px, and subsequently would yield a more accurate result compared to the original analysis without the window offset.

In principle the same method can be applied to the interrogation analysis of a single multiple-exposure image. Instead of computing the auto-correlation for a single interrogation region the cross-correlation is computed between two interrogation regions within the same image (Keane and Adrian 1993). (For the case of a zero window offset this method is identical to auto-correlation analysis.) The only difference with respect to the analysis of a single-exposure image pair is that we need to ignore the self-correlation peak (which is

Received: *29 April 1996*/*Accepted*: *29 October 1996*

J. Westerweel
Laboratory for Aero & Hydrodynamics,
Delft University of Technology,
NL-2628 AL Delft, The Netherlands

D. Dabiri, M. Gharib
Center for Quantitative Visualization,
California Institute of Technology,
Pasadena, CA 91125, USA

Correspondence to: J. Westerweel

A version of this paper was presented at the 7th International Symposium on Flow Visualization, Seattle, WA, USA, September 1995

The research of dr.ir. J. Westerweel has been made possible by a fellowship of the Royal Netherlands Academy of Arts and Sciences. The visit of dr.ir. J. Westerweel to the C.Q.V. was supported by URI(N00014-92-J-1618) from the Office of Naval Research. The authors would like to thank dr. M. Raffel for its comments and suggestions with respect to certain parts of the original manuscript.

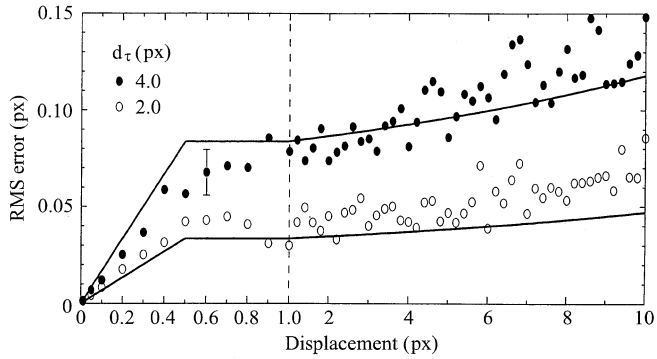

Fig. 1. The RMS estimation error for the displacement as a function of the displacement u in pixel units for a 32×32-pixel interrogation region in digital PIV cross-correlation analysis, for particle-images with a diameter of 2 and 4 pixels with an image density of 10, with zero out-of-plane displacement. The solid lines are analytical results (Westerweel 1993a, b); the symbols are obtained from Monte Carlo simulations (the error bar represents the uncertainty of the simulation result)

displaced by the window offset) when searching for the highest displacement-correlation peak.

It should be noted that cross-correlation analysis with a window offset is not new in itself: Keane and Adrian (1993) proposed to use a window offset equal to the in-plane displacement to optimize the detectability of the displacement-correlation peak with respect to the random correlation peaks (the in-plane loss-of-pairs is minimized for a window offset that equals the particle-image displacement). However, in this paper we will investigate in particular the noise reduction effect as a result of using a (discrete) window offset in the (digital) evaluation of PIV recordings.

In Sect. 2 a simple model is introduced that can be used to predict the noise reduction, based on the analytical result for the measurement error as a function of the displacement. Section 3 describes the simulations which use synthetic PIV images of isotropic turbulent flows to verify the predicted behavior. The application of the window offset method to PIV measurements in actual flows is described in Sect. 4, and in Sect. 5 we present the main conclusions from this study.

2 Theory

2.1 Signal-to-noise ratio for PIV measurements

We define the total signal power as the variance of the fluctuating displacement (viz., velocity), i.e.:

$$S = \mathrm{var}\{u\} = u'^2 \tag{2}$$

The RMS measurement error depends on the displacement, so we define the total noise power as:

$$N \equiv \int \mathrm{var}\{\varepsilon|u\}\, f(u)\, \mathrm{d}u \tag{3}$$

where $\mathrm{var}\{\varepsilon|u\}$ is the conditional variance of the measurement error ε for a given displacement u, and $f(u)$ is the probability density function (PDF) for the displacement (viz., velocity).

In order to investigate the effect of a window offset on the displacement measurement error we introduce a simple model that describes the essential characteristics of the analytical curve in Fig. 1, i.e.:

$$\mathrm{var}\{\varepsilon|u\} = \begin{cases} 4c^2u^2 & \text{for } |u| < \frac{1}{2} \\ c^2 & \text{elsewhere} \end{cases} \tag{4}$$

In Fig. 2a are sketched the estimation error and the displacement distribution that are typical for PIV interrogation analysis without window offset, i.e. the displacement u is about $\frac{1}{4}$ of the width of the interrogation window (Keane and Adrian 1993). Since: $u \gg \frac{1}{2}$px, the RMS measurement error is independent of u (viz., $\mathrm{var}\{\varepsilon|u\} = c^2$). Then, by (3) we find

$$N = \int c^2 f(u)\, \mathrm{d}u = c^2 \tag{5}$$

(by definition the integral of $f(u)$ over u is one), and subsequently the single-to-noise ratio becomes

$$\frac{S}{N} = \frac{u'^2}{c^2} \tag{6}$$

So, the SNR for PIV interrogation analysis *without* window offset is proportional to the variance of the fluctuating displacement. In other words, the displacement fluctuations in a turbulent flow can be determined with higher (relative) accuracy for increasing turbulence levels.

In the remainder of this section we will discuss the effect of window offset on the signal-to-noise ratio for the measurement of the displacement. Because of the behavior of $\mathrm{var}\{\varepsilon|u\}$ as a function of u, we will discuss two situations. First, we consider the case where the fluctuations of the displacement are smaller than $\frac{1}{2}$px. (For a normal PDF for u with $u' = 0.25$ px a fraction of 95% of the displacements has an absolute difference of less than $\frac{1}{2}$px with respect to the mean.) Subsequently, we will consider the case where the fluctuations of u are considerably larger than $\frac{1}{2}$px.

The situation for small u' would correspond to a PIV measurement of a flow with low turbulence intensity, whereas the situation with high u' to a measurement of a flow with high turbulence intensity.

2.2 Flows with low turbulence intensity

In Fig. 2b are shown sketches of the RMS measurement error and the displacement PDF for the same flow situation as in Fig. 2a, but now the interrogation analysis is carried out with a window offset that is equal to the mean displacement. The residual mean displacement is equal to zero, and the RMS estimation error is directly proportional to u (provided that the total width of $f(u)$ is less than 1 px). Now Eq. (3) yields:

$$N = 4c^2 \int u^2 f(u)\, \mathrm{d}u = 4c^2 u'^2 \tag{7}$$

The total signal power remains unchanged, i.e. $S = u'^2$, so we obtain the following expression for the signal-to-noise ratio:

$$\frac{S}{N} = \frac{u'^2}{4c^2u'^2} = \frac{1}{4c^2} \tag{8}$$

The surprising result is the SNR, by applying the window offset, no longer depends on u'; the relative measurement error is constant

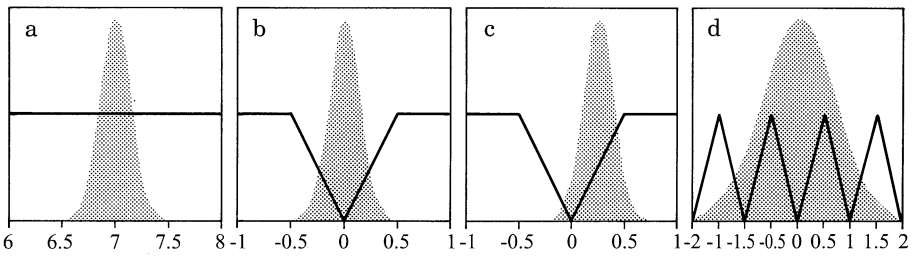

Fig. 2a–d. Schematic representation of the behavior of the measurement error (solid line) for different cases of the displacement distribution (shaded curve). **a** Without window offset; **b** with a window offset that matches the mean displacement; **c** as **b**, but now the mean displacement is not an exact integer number of pixels; **d** as **b**, but now for a high turbulence intensity

In the preceding analysis we implicitly assumed that the mean displacement is exactly an integer number of pixel units, and that the range of u is less than 1 px. Obviously, this is not generally the case (unless we deliberately design the experiment to meet these requirements). In Fig. 2c the situation is sketched for the case with a non-zero residual mean displacement. The result is that the improvement of the SNR by applying the window offset is not as large as for the case when the window offset exactly matches the mean displacement. For low turbulence intensities the effect will strongly depend on the value of the residual mean displacement, with a maximum effect for a residual mean displacement of 0, and a minimal effect for $\pm\frac{1}{2}$px. We will discuss this matter further in Sect. 3.

2.3
Flow with high turbulence intensity

For large u' (i.e., high turbulence intensity) the difference between the actual displacement and the mean displacement can be much larger than $\frac{1}{2}$ px. We therefore offset the interrogation windows by the integer part of the actual displacement (rather than the integer part of the mean displacement). This implies that the interrogation is done in two passes: First the displacement is estimated without using a window offset, and the result is used to determine the (integer) offset for the second interrogation pass. The displacement PDF and (effective) RMS measurement error for this situation are sketched in Fig. 2d.

For large u', we may assume that $f(u)$ is constant over each 1-pixel wide section of u. In that case the noise N, given by (3), can be written as

$$N \approx 4c^2 \int_{-1/2}^{1/2} u^2 \,\mathrm{d}u \sum_i f(u_i) \approx \frac{1}{3} c^2 \tag{9}$$

(Note that the summation is the first-order numerical approximation of the integral over $f(u)$, which approaches one for large u'.) Hence, for flows with a high turbulence intensity the signal-to-noise ratio for PIV measurements with window matching is expected to be approximately:

$$\frac{S}{N} \approx 3\,\frac{u'^2}{c^2} \tag{10}$$

which is three times the SNR for a PIV measurement without using a window offset; see Eq. (6).

2.4
Noise reduction

The noise reduction (NR) that is achieved by applying the window offset is defined as the ratio of the SNR for the measurement without a window offset and the SNR for the measurement with the window offset. Given Eqs. (3) and (5), the general equation for the noise reduction reads

$$\mathrm{NR} = \left[\int \frac{\mathrm{var}\{\varepsilon|u\}}{c^2} f(u)\,\mathrm{d}u \right]^{-1} \tag{11}$$

From this equation it is easily verified that if: var $\{\varepsilon|u\} < c^2$ over any interval of u, then NR > 1. Thus, interrogation analysis with a window offset will always yield a more precise result compared to the conventional analysis method.

The noise reduction in the limits of large and small u' can be easily obtained from the expressions for the SNR derived previously. For small u' the ratio of Eqs. (6) and (8) yields

$$\mathrm{NR} = \frac{1}{4u'^2} \tag{12}$$

whereas for large u' the ratio of Eqs. (6) and (10) yields

$$\mathrm{NR} \approx 3 \tag{13}$$

Note that the noise reduction in these two expressions does not depend on the value of c. Since c, which can be associated with the particle-image diameter, does not appear in Eqs. (12) and (13) implies that the noise reduction is independent of the size of the particle images.

3
Simulations

To verify the theoretical results given in the previous section a number of simulations was carried out in which we generated synthetic digital PIV images of isotropic turbulence. We investigated the noise reduction for different turbulence intensity levels and different residual displacements. We first describe the generation of the synthetic PIV images and the evaluation of the PIV data, which is followed by a discussion of the simulation results.

3.1
Generation of synthetic PIV images

Pairs of synthetic PIV images are generated from two data sets of particle locations in a rectangular volume. The locations in the first data set are generated by a random number generator. For each particle we carry out a Lagrangian integration for a given velocity field over a given time period, and the final locations for all particles constitute the second set of particle locations. The velocity field for the integration in generated by the method of 'kinematic simulation' (Fung et al. 1992), which

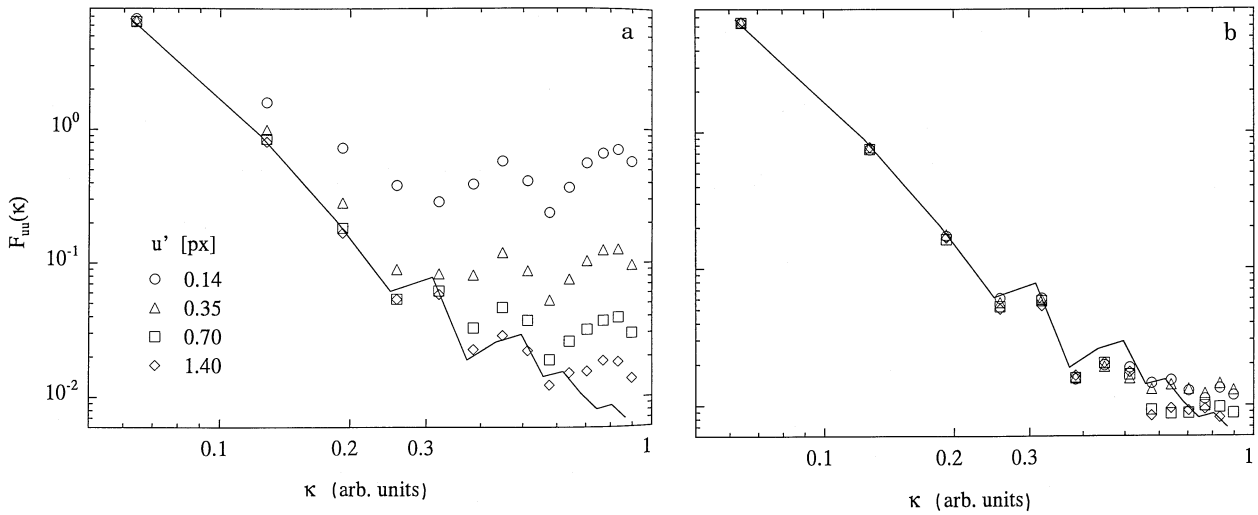

Fig. 3a, b. The power spectra for turbulence intensities u' of 0.14, 0.35, 0.70 and 1.40 px, normalized by u', without window offset **a** and with window offset **b** for synthetic PIV images of isotropic turbulence. The solid lines represent the power spectra of the actual flow field

yields a velocity field with the kinematic characteristics of isotropic turbulence. The length of the integration period determines the turbulence intensity, and a constant displacement is added to account for a uniform advection of the flow.

Each particle is assigned a brightness value according to its location within a virtual light sheet with a Gaussian intensity profile. We assume that the continuous images of all particles have a (two-dimensional) Gaussian shape: the pixel gray values of the discrete images are found by integration of the continuous image for each pixel. All synthetic images have a resolution of 512×512 pixels and have an image density of 10 particle images per 32×32-pixel interrogation sub-image, with a mean in-plane displacement of 7 px and a particle-image diameter of 4 px.

Each pair of synthetic PIV images is analyzed by computing the image cross-correlation in 32×32-pixel sub-images with a 50% overlap between adjacent interrogation regions. This yields a data set of 31×31 displacement vectors per image pair. We evaluate the results by computing for each data set the one-dimensional power spectra of the fluctuating displacement field. (Since the statistics of the simulated flow field are homogeneous, we can compute the spectrum for each row of data, and then average over all rows.) We also computed the velocity power spectrum of the actual velocity field. From the spectra we can easily evaluate the SNR: the signal power S (by definition) is equal to the square of u', which is an input parameter for the simulation; the noise N is determined by integration of the difference of the measured spectrum and the actual spectrum.

3.2
Influence of turbulence intensity

We first generated a set of image pairs with a mean in-plane displacement of exactly 7 pixels, and with turbulence intensities of 0.14, 0.35, 0.70 and 1.40 px (corresponding to turbulence levels of 2%, 5%, 10%, and 20% respectively). The results for the power spectra normalized by the squared turbulence intensities are plotted in Fig. 3. The solid line in this figure represents the spectrum of the actual flow field. (The spectrum is not smooth because we only observe a single realization of the flow field; the expected scaling behavior, i.e. $F_{uu}(\kappa) \sim \kappa^{-5/3}$, is only found for the ensemble average over many realizations of the flow field.) The symbols denote the results from the synthetic PIV images.

Figure 3a shows the results for the interrogation analysis of the synthetic images without window offset. For the lowest value of u' the measured spectrum already deviates from the actual spectrum at very small wavenumber and the actual velocity spectrum can only be resolved over a very small fraction of the total available wavenumber range. As u' increases the measurement noise decreases relative to the signal, and thus the range over which the actual spectrum can be resolved increases. At the highest value of u' that was simulated the actual velocity spectrum could be determined over almost the complete range of wavenumbers. It is clear that the influence of the measurement noise for the interrogation analysis without window offset decreases with increasing u', as predicted by Eq. (6).

The results for the interrogation analysis of the same synthetic images, but now with window offset, are shown in Fig. 3b. Equation (8) predicted that the SNR would be independent of u'. Indeed, the results show that for all simulations the wavenumber range over which the spectrum could be determined is practically identical for all image pairs. In particular the difference in the results for the lowest value of u' that was simulated is quite remarkable: without a window offset the velocity spectrum could be determined only for the lowest wavenumbers, whereas with the window offset the spectrum could be determined over almost the full wavenumber range.

In Fig. 4 we plotted the noise reduction as a result of the window offset as a function of the turbulence level in the simulations. The solid line represents the noise reduction for small u'. ref. Eq. (12), whereas the dotted line represents the noise reduction of 3 in the limit of large u', ref. Eq. (13).

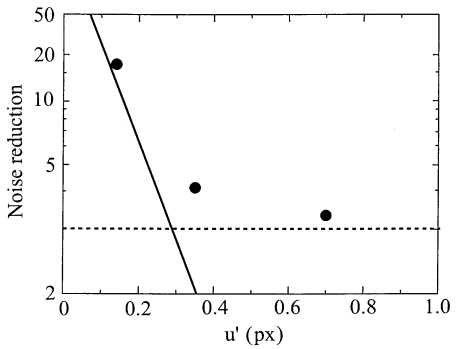

Fig. 4. The noise reduction as a function of the RMS fluctuating displacement u' (in pixel units). The solid line is the predicted noise reduction for small u'; the broken line is the predicted reduction for large u'. The symbols represent the results from synthetic PIV images of isotropic turbulence. (Note that the noise reduction is plotted against a non-linear axis, so that the solid line appears as a straight line)

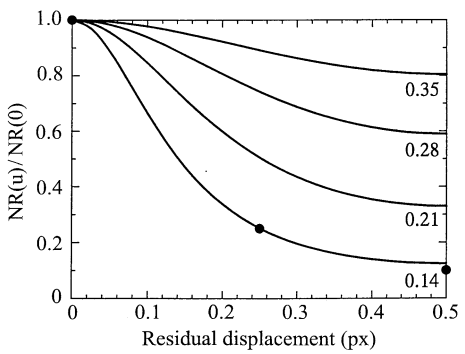

Fig. 5. The noise reduction as a function of the residual mean displacement $\bar{u}$ normalized by the noise reduction for $\bar{u}=0$ for different values of the RMS fluctuating displacement u' (in pixel units), as predicted by the model described in Sect. 2. The symbols represent the results from synthetic PIV images of isotropic turbulence with $u'=0.14$ px

3.3
Influence of non-zero residual displacement

In a second set of simulations we analyzed synthetic PIV image pairs with $u'=0.14$ px and mean displacements of 7.00, 7.25 and 7.50 px, i.e. with residual mean displacements of 0.00, 0.25 and 0.50 px respectively. We first interrogated these image pairs without window offset, and subsequently the same image pairs but now with a window offset of 7 px. The results for the noise reduction, determined in the same way as in the previous simulations, are plotted in Fig. 5. We also plotted in this figure the noise reduction as a function of the residual displacement for different values of u' as predicted by the model described in Sect. 2. The results from the previous set of simulations showed that we can achieve a considerable noise reduction by applying the window offset. However, the results in Fig. 5 show that this will only be achieved when the residual displacement is close to zero. As u' increases, the dependence of the noise reduction on the residual displacement becomes less prominent. So, for large u' the noise reduction approaches a value of 3 (independent of the value of the residual displacement).

4
Experimental

Evidently, the theoretical model presented in Sect. 2 and the simulations described in Sect. 3 deal with idealized circumstances that may not be encountered in a practical situation. In this section we describe two experiments in which we applied the window offset: the measurement of grid-generated turbulence and that of fully-developed turbulent pipe flow.

4.1
Grid-generated turbulence

The PIV measurements of grid-generated turbulence are carried out in a closed-loop water channel with a cross-section of 15×15 cm^2. The mean flow velocity is 272 mm/s, and the turbulence is generated by a perforated plate with a mesh size of 4 mm and a solidity of 0.25. The images are recorded at a distance of 160 mm (i.e., 40 grid-mesh lengths) downstream from the grid; at this location the turbulence intensity is about 2.5% of the mean velocity. At the same location we also took measurements with laser-Doppler velocimetry, using a two-component (488 and 514 nm) dual-beam back-scatter configuration with a beam separation and lens focal length of 38 and 400 mm respectively.

The flow was seeded with 14 μm particles with a specific gravity of 1.4 g/cm^3 at a number density of 8 mm^{-3}. Images are recorded with a high-speed 768×480-pixel CCD camera (Dantec). A total of 60 digital image pairs is recorded of a 45×33 mm^2 area in the flow, illuminated by a 1 mm thick light sheet that is created by expanding the beam of a 3 W Ar^+ laser. The plane of the light sheet coincides with the centerline of the channel, and is parallel with the transparent wall between the light sheet and the camera. The exposure time and time delay for the image pairs are 1.500 and 0.250 ms respectively. The mean velocity corresponds to a 7.1 px displacement. The RMS fluctuating displacement (viz., u') is 0.18 px (i.e., 2.5% of the mean displacement), which implies that all the displacements due to the turbulence are less than the size of a pixel. The particle-image diameter was estimated at 3.6 px, so for c we expect a value of about 0.1 px (see Fig. 1).

Each pair of images is interrogated using cross-correlation analysis in 32×32-pixel sub-images with an overlap of 50% between adjacent interrogations, which yields a total of 1363 vectors per image pair. The arrow plot in Fig. 6a shows the measured displacement relative to the mean displacement (indicated by the large arrow at the top) interrogated without window offset. With $u'=0.18$ px and $c\approx0.1$ px, the SNR for this result is estimated at about 3. The turbulent character of the flow is visible, but clearly influenced by the presence of measurement noise.

Applying a window offset of 7 px, and repeating the analysis for the same set of images, yields the result shown in Fig. 6b. The window offset has reduced the measurement noise considerably. We would like to emphasize that the smooth appearance of the data in Fig. 6b is the result of the noise reduction and *not* the result of any kind of spatial filtering.

The large data set (i.e., 60 frame pairs, each yielding 29 lines of 47 vectors each) allows us to make meaningful estimates of

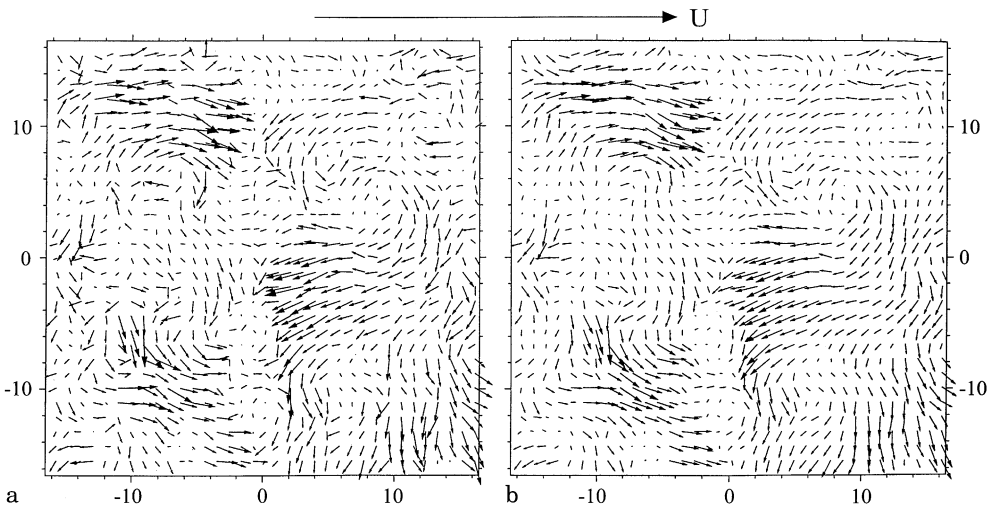

Fig. 6a, b. Arrow plots of the fluctuating displacement for a turbulent flow behind a grid, without **a** and with **b** window offset. The mean displacement is indicated by the reference arrow at the top. The axis scales are in mm. (Note: the displacements have been scaled with a factor of 65 with respect to the dimensions of the plot axes.)

the turbulent velocity power spectra, and compare the results with and without application of a window offset. The spectra are determined by computing the spectrum for each row of velocity data in the streamwise direction, and then ensemble averaging over all rows of data and all images. (We have assumed here that the velocity statistics are homogeneous within the view area of the camera.) The results for the spectra normalized by the Taylor microscale, denoted by λ, are plotted in Fig. 7. We also determined the velocity power spectrum from the measurements with LDV, which have been included in Fig. 7.

The results in Fig. 7 show that the measurement noise dominates the spectrum for $\kappa\lambda > 2$. The result for the spectrum determined from the data obtained with the window-offset interrogation compares quite well with the LDV result. The measurement noise no longer makes a significant contribution to the result for the measured spectrum.

We also plotted in Fig. 7 the result for the spectrum obtained from hot-wire measurements by Comte-Bellot and Corrsin (1971) in grid-generated turbulence at a distance of 45 grid-mesh lengths behind the grid. Our measurements agree quite well with those of Comte-Bellot and Corrsin. It should be noted that the small differences that remain could be related to differences in the experimental facilities.

The constant noise level at large wavenumbers in Fig. 7 corresponds to a SNR of 3.6. Given that $u' = 0.18$ px, the RMS measurement error for the displacement is 0.095 px (cf., Fig. 1). This value corresponds quite well with our *a priori* estimate of $c \sim 0.1$ px. Equation (12) predicts a noise reduction of 7.7 for $u' = 0.18$ px with zero residual displacement; the noise reduction for a 0.1 px residual displacement is 80% of the noise reduction at zero residual displacement (see Fig. 5). Hence, the expected noise reduction is: $(0.8 \times 7.7 =) 6.2$. This value compares quite well with the reduction of the measured PIV spectra at high wavenumbers as can be observed in Fig. 7. Hence, the SNR for the result obtained with interrogation analysis with window offset is estimated at: $(6.2 \times 3.6 =) 22.3$, which implies an average measurement error of about 0.04 px.

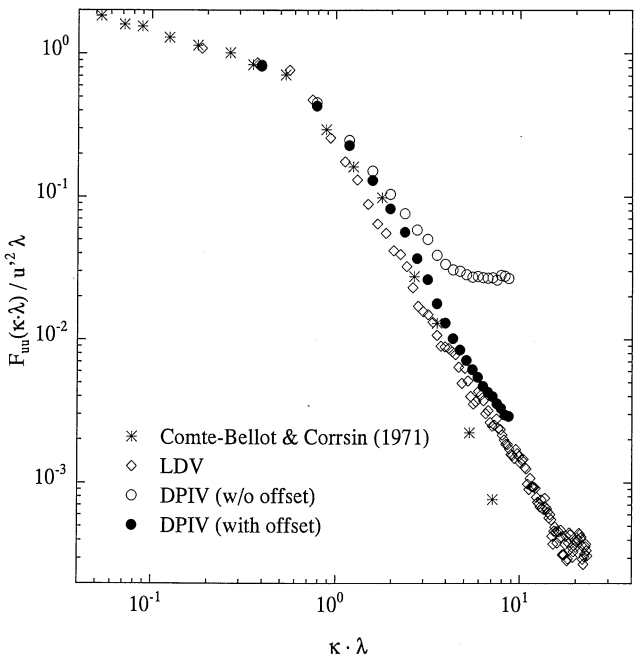

Fig. 7. The normalized power spectrum of the fluctuating streamwise velocity of a turbulent flow behind a grid (at 40 grid-mesh lengths away from the grid). The open dots represent the result obtained with PIV without window offset; the closed dots the same image data but now with window offset. Also plotted are the result obtained with LDV ($\diamond$) in the same facility and at the same location as for the PIV, and the result obtained with hot-wire anemometry ($\times$) by Comte-Bellot and Corrsin (1971)

4.2
Fully-developed turbulent pipe flow

The kinematic characteristics of a turbulent flow behind a grid are very close to that of the flow field generated by the kinematic simulation. It may therefore not be too much of

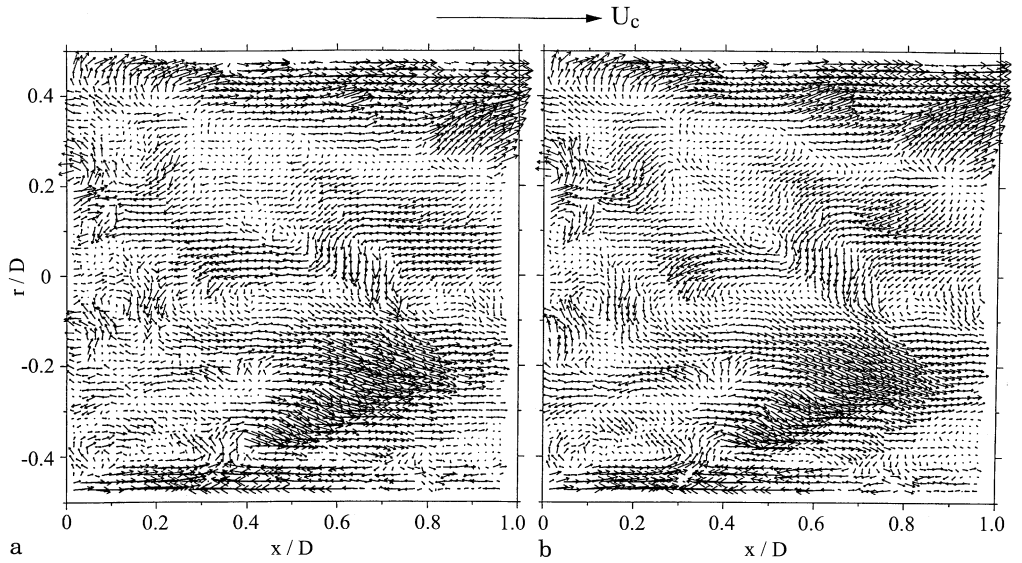

Fig. 8a, b. Arrow plots of the fluctuating displacement relative to the mean velocity profile for a fully-developed turbulent pipe flow from a multiple-exposure PIV recording. **a** The result obtained with auto-correlation analysis; **b** the result with cross-correlation analysis with offset interrogation windows. The mean displacement at the centerline (i.e., 12 px) is indicated by the reference arrow at the top. (Note: the displacements have been scaled by a factor of 30 with respect to the dimensions of the plot axes.)

a surprise to find such a good agreement between the results from the simulations and those from the grid-turbulence measurements. To investigate whether the noise reduction can also be found in other experiments we analyzed an existing set of digital PIV images of a fully-developed turbulent pipe flow. An important difference with respect to the previous experiment, apart from the flow itself, is that the pipe flow images were recorded with multiple exposures per image. A detailed description of the pipe flow measurements is given by Westerweel et al. (1996), and we therefore limit ourselves here to a very brief description of the experiment.

The measurements were carried out in a water-filled pipe with a diameter of 40 mm, at a Reynolds number of 5300 (based on the pipe diameter and the bulk velocity). A total of 100 images was recorded of an area that covered the full diameter of the pipe, using a 1000×1016-pixel CCD camera. The time between exposures was 2.685 ms and the total recording period for each image was 15 ms, so each image was exposed five times. In total 100 images were recorded at a rate of 1 Hz (the integral time scale of this flow is about 0.3 s).

In the original measurement, these images were analyzed by computing the image auto-correlation in 32×32-pixel interrogation regions. This time we used cross-correlation interrogation analysis by extracting two interrogation sub-images from the same (multiple-exposed) image, and used the results from the original analysis (i.e. without using a window offset) to determine the window offset at every individual interrogation position.

Figure 8 shows the results from the original analysis without the window offset and the present analysis with the window offset. The signal-to-noise ratio at the centerline of the pipe for the original measurement was estimated at 25 (i.e., $u' \approx 0.6$ px, $c \approx 0.12$ px; see Westerweel et al. 1996). On the whole, the result of the analysis with window offset shows a reduction of the measurement noise. However, to fully appreciate the improvement of the SNR achieved by the window offset we need to zoom in on the results: comparing the details in Fig. 9, which are taken from the arrow plots in Fig. 8, shows that the noise reduction effected by the window offset made it possible

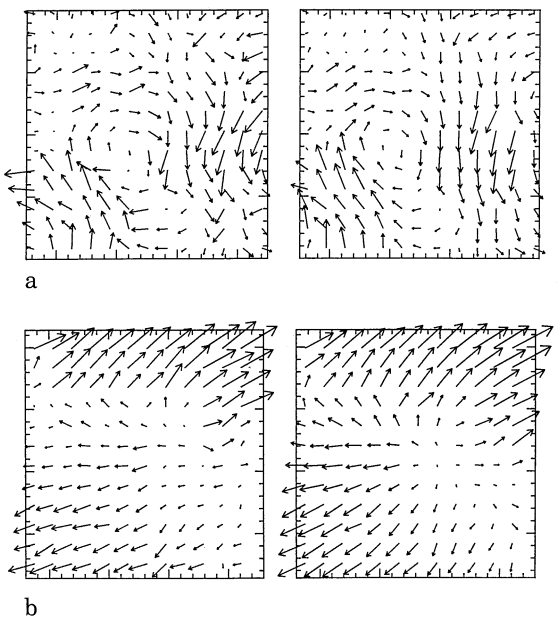

Fig. 9a, b. Details from the arrow plots of Fig. 8. **a** $(x, r) = (0.13D, -0.05D)$; **b** $(x, r) = (0.88D, 0.21D)$. The area for each arrow plot is $0.2D \times 0.2D$. The left arrow plot of each pair shows the original result; the right plot shows the result for the analysis with window offset

to observe flow structures that would otherwise remain practically undetected.

In order to evaluate the noise reduction quantitatively we need to determine the velocity power spectra. For this purpose we make use of the fact that the turbulence statistics for pipe flow are homogeneous along the axis direction. So, the spectrum at a given radial distance from the centerline could be determined by computing the spectrum for each row of data, and then ensemble averaging the spectra for identical radial positions over all images. The results for the spectra at radial distances of 0.00, 0.25 and 0.45 pipe diameters (D) from the centerline are shown in Fig. 10.

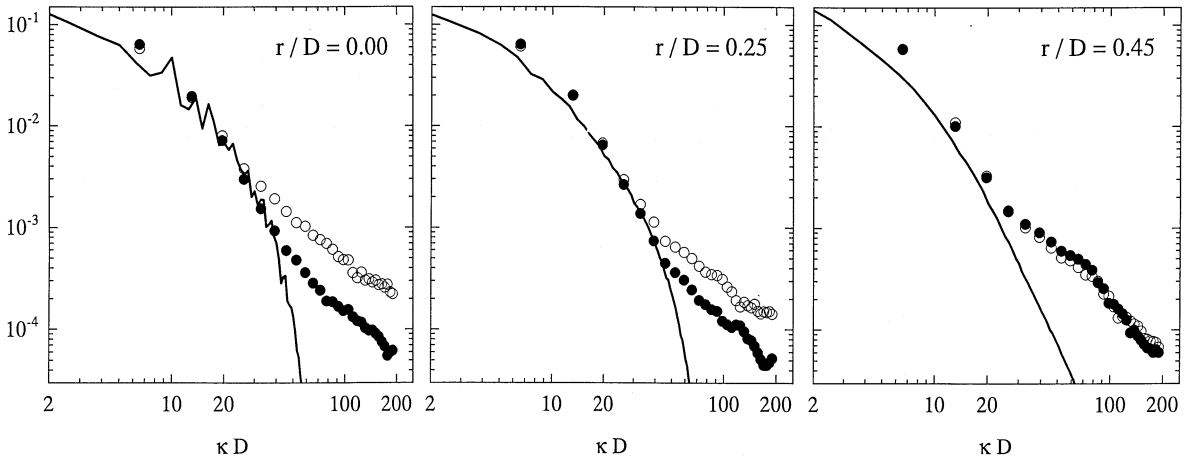

Fig. 10. The power spectra for the axial velocity component measured with DPIV in a fully-developed turbulent pipe flow at 0.00, 0.25 and 0.45 pipe diameters from the centreline of the pipe. The open symbols represent the results without window offset, the closed symbols the results with window offset; the solid lines are the spectra obtained from a direct numerical simulation

The mean axial displacements at $r/D = 0.00$, 0.25 and 0.45 are equal to 11.7, 10.6 and 6.9 px respectively, and the RMS fluctuating axial displacements are equal to 0.6, 0.8 and 1.7 px respectively. Since the RMS fluctuating displacements are all larger than 0.5 px, we expect a noise reduction of about 3 (see Fig. 4). The spectra at $r/D = 0.00$ and 0.25 indeed show a noise reduction of about 3. As a result, the range of wavenumbers over which the numerical and experimental spectra agree is slightly larger for the results with window offset. However at $r/D = 0.45$ there is no visible effect; we think this may be attributed to the strong velocity gradients very close to the pipe wall; strong velocity gradients tend to split up the displacement-correlation peak, which is an additional source of error in the estimation of the displacement that is not taken into account in the model described in Sect. 2.

5
Discussion and conclusions

The results presented in this paper show the use of a window offset that is equal to the (integer part of the) displacement (in pixel units) reduces the noise level of the measurement. In other words, the use of a window offset optimizes the performance for the estimation of the displacement. We used a simple model to predict the effect as a function of the variation of the fluctuating displacement. The effect was demonstrated in the analysis of synthetic PIV images of isotropic turbulence, and in actual measurements of grid-generated turbulence and of fully-developed turbulent pipe flow.

The theoretical analysis and simulations show that the noise reduction is always larger than one, and that the magnitude of the noise reduction depends on the variation of the fluctuating displacement, i.e. u'. For large u' the noise reduction is independent of u', with an average value of 3; for small u' the noise reduction is directly proportional to u'^2. In particular situations (i.e. if the mean displacement is near an integer number of pixel units) the noise reduction can be quite large, as demonstrated in the simulations and in the measurement of grid-generated turbulence.

We have seen that the noise reduction is inversely proportional to u' (i.e., the turbulence intensity of the velocity field). So, the method is particularly useful to improve the signal-to-noise ratio for measurements of weak turbulence. Earlier, Hinsch et al. (1987) and Raffel and Kompenhans (1994) used image shifting to compensate for the uniform displacement of particle images, while extending the exposure time delay; in this way the variation of the fluctuating displacement is increased with respect to the variation of the measurement error, while at the same time the particles remain within the interrogation region. The noise reduction that is achieved by image shifting is proportional to the factor by which the time delay is extended. For interrogation analysis with window offset the SNR is independent of the value of u' (for small u'), and thus also independent of the time delay. The noise reduction (with respect to the interrogation result without window offset) is achieved without extending the exposure time-delay. This means that we are less likely to violate the requirement for 'frozen turbulence'.

From the results of the grid-turbulence measurements we concluded that the average measurement error for the interrogation analysis with the window offset was about 0.04 px. If the absolute displacement of the particles is 8 px (i.e., $\frac{1}{4}$th of the diameter of a 32×32-pixel interrogation window) then this would imply a relative measurement error of 0.5%. One might question whether this is also a realistic measure for the overall measurement accuracy; in practice, optical distortions and uncertainties in the image magnification and exposure time-delay might be larger than the relative measurement error for the particle-image displacement. Since the variation of ε depends on both the particle-image diameter and the size of the interrogation region (Westerweel 1993a, b). we may combine the window offset with a reduction of the window size in such a way that the variation of the measurement error remains at a constant level. Hence, interrogation with window offset and with reduced interrogation window size would yield a result with an improved spatial resolution (since we reduced the size of the interrogation region) at the same signal-to-noise ratio in comparison to the interrogation analysis without window

offset. We could thus apply the window offset to improve the spatial resolution of the measurement.

Finally, we would like to emphasize that the application of a window offset in the interrogation analysis does not require any special techniques at the time of image recording, and it applies to both pairs of single-exposure images and multiple-exposure images. Only a few minor adaptations to the analysis software are required. The noise reduction, so to speak, 'comes for free.'

References

Adrian RJ (1991) Particle-imaging techniques for experimental fluid mechanics. Annu Rev Fluid Mech 22: 261–304

Comte-Bellot G; Corrsin S (1971) Simple Eulerian time correlation of full and narrow-band velocity signal in grid-generated, 'isotropic' turbulence. J Fluid Mech 48: 273–337

Fung JCH; Hunt JCR; Malik NA; Perkins RJ (1992) Kinematic simulation of homogeneous turbulence by unsteady random Fourier modes. J Fluid Mech 236: 281–318

Hinsch K; Arnold W; Platen W (1987) Turbulence measurements by particle imaging velocimetry. Pages 127–134 of: Stevenson, WH (ed), ICALEO '87 — Optical Methods in Flow and Particle Diagnostics. Toledo OH: Laser Institute of America

Keane RD; Adrian RJ (1993) Theory of cross-correlation of PIV images. Nieuwstadt FTM (ed). Flow Visualization and Image Analysis. Dordrecht: Kluwer Academic, pp 1–25

Prasad AK; Adrian RJ; Landreth CC; Offutt PW (1992) Effect of resolution on the speed and accuracy of particle image velocimetry interrogation. Exp Fluids 13: 105–116

Raffel M; Kompenhans J (1994) Error analysis for PIV recording utilizing image shifting. Proc 7th Int. Symp Appl Laser Techn Fluid Mech (Lisbon, 11–14 July 1994) p. 35.5

Westerweel J (1993a) Analysis of PIV interrogation which low pixel resolution. Pages 624–635 of: Cha SS; Trolinger JD (eds). Proc SPIE-2005. Optical Diagnostics in Fluid and Thermal Flow. (San Diego, 14–16 July 1993)

Westerweel J (1993b) Digital Particle Image Velocimetry — Theory and Application. Ph.D. thesis. Delft University of Technology, the Netherlands

Westerweel J; Draad AA; Van der Hoeven JG Th; Van Oord J (1996) Measurement of fully-developed turbulent pipe flow with digital PIV. Exp Fluids 20: 165–177

Willert CE; Gharib M (1991) Digital particle image velocimetry. Exp Fluids 10: 181–193